Recent progress on modeling nonlinear wave propagation and wave-structure interaction using a high-order shifted boundary method: Capabilities, challenges, and perspectives

Jens Visbech[1], **Allan P. Engsig-Karup**[1], **Harry B. Bingham**[2], **Mario Ricchiuto**[3]
[1] Dept. of Applied Mathematics, Technical University of Denmark, Denmark
[2] Dept. of Civil & Mechanical Eng., Technical University of Denmark, Denmark
[3] Team CARDAMOM, INRIA, U. Bordeaux, CNRS, Bordeaux, France
Email to the corresponding author: jvis@dtu.dk

INTRODUCTION

In a previous workshop, IWWWFB39, a high-order shifted boundary method for water waves and floating bodies was presented in [1]. This abstract reports recent progress on modeling nonlinear wave propagation and wave-structure interactions with this numerical approach. The purpose is to highlight current capabilities, challenges, and perspectives of using this unfitted technique for ocean wave modeling. Considering nonlinear potential flow solved with a finite or spectral element method, the free surface is curved, deforming, and moving in time. Additional complex boundaries, such as bathymetry or bodies, make mesh handling difficult, requiring costly re-meshing or updating at each time step. An unfitted boundary approach can avoid this by approximating the domain on a simple background mesh, avoiding all re-meshing issues. The main challenge is to correctly impose the boundary conditions on the unfitted domain. Here, we employ the shifted boundary approach [2], which enables us to represent curved features and retain high orders, while mitigating the *small-cut-cell* issue commonly found in classical embedded methods, [3]. We first review the flow equations and recall the shifted boundary formulation after [1]. We then present a selection of results and discuss the open challenges.

GOVERNING EQUATIONS

Given a fluid domain Ω enclosed by its boundaries: the bathymetry Γ^{b}, rigid walls Γ^{w}, periodic boundaries Γ^{p}, body surfaces Γ^{body}, and the free surface Γ^{η}. Assuming potential flow, the velocity field $\boldsymbol{u} = (u, w)$ is defined by $\boldsymbol{u} = \boldsymbol{\nabla}\phi$ with $\boldsymbol{\nabla} = (\partial_x, \partial_z)$. We seek $\phi \in C^2(\Omega)$ to solve the Laplace problem

$$\boldsymbol{\nabla}^2\phi = 0 \quad \text{in} \quad \Omega \times \mathcal{T}, \quad \phi = \phi_\eta \quad \text{on} \quad \Gamma^\eta \times \mathcal{T}, \quad \boldsymbol{\nabla}\phi \cdot \boldsymbol{n} = q_i \quad \text{on} \quad \Gamma^i, \tag{1}$$

where $\mathcal{T} : t \geq 0$ is the time domain and $\boldsymbol{n} = (n_x, n_z)$ the outward normal. Here, q_i for $i \in \{\mathrm{b}, \mathrm{w}, \mathrm{body}\}$ denotes the boundary flux, with $q_i = 0$ for impermeable and $q_i = q_i(t) \neq 0$ for moving boundaries. Periodic conditions on Γ^{p} are imposed by folding the domain. Combined with (1) are the nonlinear free-surface conditions on $\Gamma^\eta \times \mathcal{T}$ as

$$\partial_t\eta = -\partial_x\eta\partial_x\phi_\eta + w_\eta(1 + \partial_x\eta\partial_x\eta), \quad \partial_t\phi_\eta = -g\eta - \frac{1}{2}\partial_x\phi_\eta\partial_x\phi_\eta + \frac{1}{2}w_\eta^2(1 + \partial_x\eta\partial_x\eta). \tag{2}$$

POLYNOMIAL-CORRECTED SHIFTED BOUNDARY FORMULATION

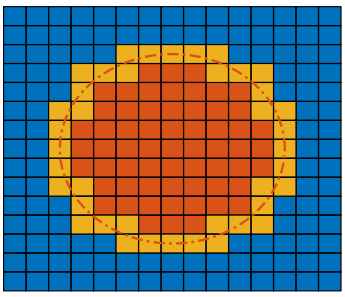

Figure 1: Domain with embedded circle. $\mathcal{C}_{\text{in}}$: $\mathcal{C}_{\text{out}}$: $\mathcal{C}_{\text{on}}$:

The shifted boundary method (SBM) was first proposed by Main & Scovazzi [2] to solve boundary value problems with finite elements. Since then, numerous studies have applied this unfitted method to various problems. The main idea is to embed the *true* domain Ω into a regular affine mesh $\mathcal{C}$. Based on a level set of the true boundary $\Gamma = \partial\Omega$, elements are classified as inside $\mathcal{C}_{\text{in}}$, outside $\mathcal{C}_{\text{out}}$, or intersected $\mathcal{C}_{\text{on}}$, such that $\mathcal{C} = \mathcal{C}_{\text{in}} \cup \mathcal{C}_{\text{out}} \cup \mathcal{C}_{\text{on}}$. The *surrogate* domain and boundary, $\overline{\Omega}_h$ and $\overline{\Gamma}_h = \partial\overline{\Omega}_h$, are then formed by selecting $\mathcal{C}_{\text{in}}$ together with none, some or all of $\mathcal{C}_{\text{on}}$. To impose boundary conditions on $\overline{\Gamma}_h$, a mapping $\mathcal{M}(\overline{\boldsymbol{x}}) : \overline{\Gamma}_h \mapsto \Gamma$ is introduced between the points $\overline{\boldsymbol{x}} = (\overline{x}, \overline{y}) \in \overline{\Gamma}_h$ and $\boldsymbol{x} = (x, y) \in \Gamma$. Combined with this mapping, Taylor series expansions are used to satisfy boundary conditions and maintain optimal convergence. For brevity, we state the final formulation of (1) as given in [1], following [4]. This form employs a polynomial correction to avoid explicitly evaluating higher-order terms in the Taylor expansion [5] and uses an Aubin-type penalty to weakly impose boundary data as

$$\begin{aligned}(\boldsymbol{\nabla}\phi, \boldsymbol{\nabla}v)_{\overline{\Omega}_h} + \tau(\phi(\boldsymbol{x}), v)_{\overline{\Gamma}_h^\eta} - (\boldsymbol{\nabla}\phi \cdot \overline{\boldsymbol{n}}, v)_{\overline{\Gamma}_h^\eta} + \overline{n}_n(\nabla(\phi(\boldsymbol{x}) - \phi) \cdot \boldsymbol{n}, v)_{\overline{\Gamma}_h^i} \\ - \overline{n}_t(\nabla\phi \cdot \boldsymbol{t}, v)_{\overline{\Gamma}_h^i} = \tau(\phi_\eta, v)_{\overline{\Gamma}_h^\eta} + \overline{n}_n(q_i, v)_{\overline{\Gamma}_h^i},\end{aligned} \tag{3}$$

where $(a, b)_c = \int_c a \cdot b \; dc$ denotes the inner product over c, and v is a test function. An implicit summation over $i \in \{\text{b}, \text{w}, \text{body}\}$ is used. Here τ is a problem-dependent penalty parameter, and $\overline{\boldsymbol{n}}$ is the outward normal on $\overline{\Gamma}_h$. Furthermore, $\overline{n}_n = \overline{\boldsymbol{n}} \cdot \boldsymbol{n}$ and $\overline{n}_t = \overline{\boldsymbol{n}} \cdot \boldsymbol{t}$, with $\boldsymbol{t}$ being the true boundary tangent. Since $\boldsymbol{x} = \mathcal{M}(\overline{\boldsymbol{x}})$, the basis functions defined on $\overline{\Omega}_h$ are evaluated on Γ. Finally, to solve (3) combined with (2) weakly, a high-order spectral element method (SEM) is employed [6].

CAPABILITIES

Forced submerged cylinder: We consider a vertically forced cylinder and compare the results to the harmonic-reconstructed data of [7] (large-amplitude motion, nonlinear force, linearized free-surface conditions). We target a motion amplitude of $A/R = 1.0$ [-], with R the cylinder radius, and an oscillation wave number $kR = 1.0$ [-]. The domain is stretched to mimic an infinite extent and avoid wave reflections: $x \in [0, 100R]$ and $z \in [-30R, 0]$, with the center of the cylinder at $(x_0, z_0) = (50R, -3R)$. Approximately 40 unfitted elements of order $p = 3$ constitute $\overline{\Gamma}_h^{\text{body}}$ at any time. The mesh has $N_x = N_z = 35$ elements. The model is ramped up linearly over one oscillation period. Figure 2 shows the vertical force $\boldsymbol{F}(t) = (F_x(t), F_z(t)) = -\rho \int_{\Gamma^{\text{body}}} \left(\partial_t\phi + \frac{1}{2}\boldsymbol{\nabla}\phi \cdot \boldsymbol{\nabla}\phi\right)\boldsymbol{n} \, d\Gamma^{\text{body}}$, with ρ the fluid density. Here, $\partial_t\phi$ is computed using an acceleration potential to reduce spurious spikes caused by time-varying truncation errors in ϕ, [1]. A visual comparison shows good agreement between the

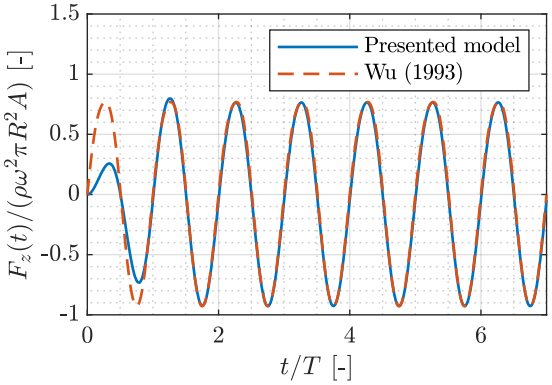

Figure 2: Force signal for a submerged vertically forced cylinder.

numerical and analytical results. Based on experience, the spurious spikes are significantly reduced compared to finite difference stencils.

Soliton propagating over a cylinder: We consider a solitary wave with height $a/h = 0.177$ [-], where $h = 0.4$ m. The domain is $x \in [0, L]$ and $z \in [-h, 0]$, with $L = 45$ m. The soliton is initially placed at $x_i = L/3$, and a cylinder of size $R/h = 0.15875$ [-] is submerged at $(x_0, z_0) = (2L/3, -h/2)$. The simulation uses an initial mesh of $N_x = 70$ and $N_y = 35$ elements of order $p = 4$, stretched to cover the full x-range with higher resolution around x_0, resulting in approximately 80 unfitted elements forming $\overline{\Gamma}_h^{\text{body}}$. Normalized forces are shown in Figure 3, compared to the boundary-fitted SEM results of [8] as a function of the relative collision time $t - t_0$. Differences between solutions are noted and are subject to further investigation. These differences are likely related to the large relative distance between Γ^η and $\overline{\Gamma}_h^\eta$, which is due to the inclusion of the cylinder that dictates the local resolution. Approximately five element lengths separate Γ^η and $\overline{\Gamma}_h^\eta$, introducing additional extrapolation errors when projecting from $\overline{\Gamma}_h^\eta$ to Γ^η, that could dampen the wave.

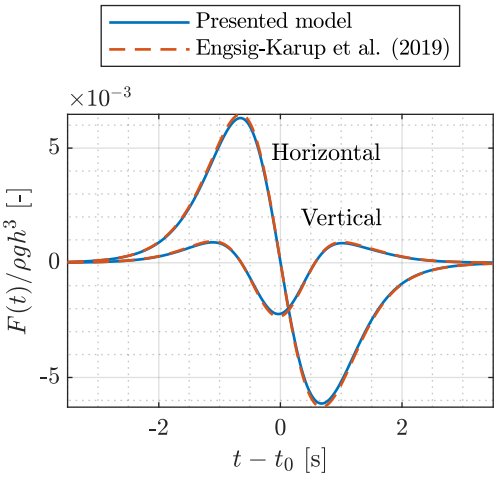

Figure 3: Cylinder force due to soliton.

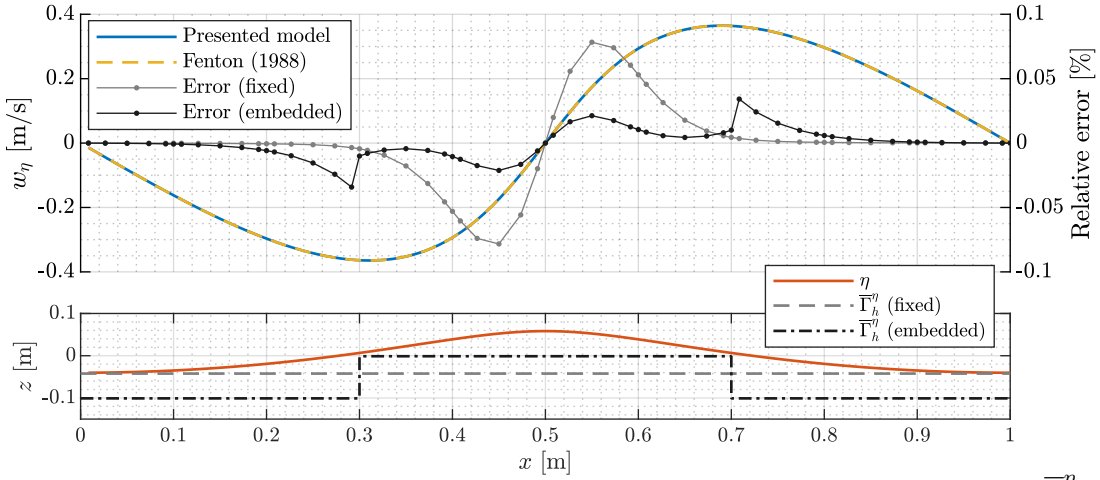

Figure 4: Simple test showcasing relative errors in w_η for fixed and embedded $\overline{\Gamma}_h^\eta$.

CHALLENGES

The main challenge concerns the embedding of Γ^η and the formation of $\overline{\Gamma}_h^\eta$. We denote $\overline{\Gamma}_h^\eta$ as *fixed* when the surrogate boundary: i) is time-invariant, ii) forms a straight vertical line, and iii) lies below $\min(\eta)$ at all times. In contrast, $\overline{\Gamma}_h^\eta$ is *embedded* when the surrogate boundary is formed as previously described in Figure 1. The embedded case, especially under mesh refinement, consists of many "jumps" similar to a staircase. These jumps induce near-discontinuous errors in w_η in (2). Multiple gradients are evaluated, amplifying these small but discontinuous errors, which can cause temporal numerical instability over time. To illustrate this, a simple test compares errors in fixed and embedded scenarios of $\overline{\Gamma}_h^\eta$ against the highly accurate periodic stream function solution of [9]. A wave with $kh = \pi$ and 70%

of maximum steepness is considered on a uniform mesh with $N_x = 10$, $N_y = 5$ elements, and order $p = 6$. In Figure 4, for the embedded case, the discontinuities appear at $x = \{0.3, 0.7\}$ m, matching the jumps of $\overline{\Gamma}_h^\eta$. The error in the fixed case is smooth. Overall, both approaches yield low relative errors of $\mathcal{O}(0.1\%)$ and are numerically convergent (not shown). Both allow p-refinement, while only the embedded option permits true h-refinement. **Remark:** All results shown in Figures 2 and 3 use a fixed free surface surrogate boundary.

PERSPECTIVES

Gradient recovery: To address the instability caused by an embedded free surface, we are investigating methods to compute $w = \partial_z \phi$ and project it onto Γ^η, ensuring smooth and stable solutions.

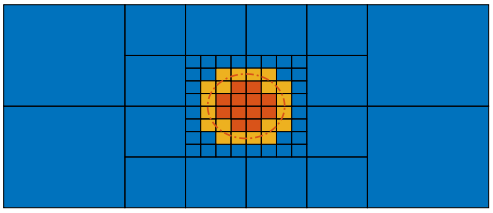

Figure 5: Non-conformal mesh with higher resolution near cylinder.

Non-conformal elements: The inclusion of structures dictates the resolution throughout the domain, based on the body's length and curvature scale. With classical conformal, body-fitted finite elements, unstructured elements are used with graded mesh refinement in the required areas [8]. The presented unfitted approach aims to use regular, easy-to-generate meshes, which conflicts with this. A possible solution is to employ non-conforming elements as a simple post-processing step on a coarse mesh, as shown in Figure 5, where a 2×4 mesh is refined around an embedded cylinder. Typically, only 2-4 elements in the vertical (depth) direction are needed for pure wave propagation. Current work focuses on integrating this meshing technique with the model presented to improve the results shown, especially for the soliton, where the distance between Γ^η and $\overline{\Gamma}_h^\eta$ (relative to the size of the elements) can be reduced.

REFERENCES

[1] Visbech, J., Engsig-Karup, A. P., Bingham, H. B., Amini-Afshar, M., and Ricchiuto, M. A high-order shifted boundary method for water waves and floating bodies. In *Proceedings of IWWWFB39* (2024).

[2] Main, A., and Scovazzi, G. 2018. *The shifted boundary method for embedded domain computations. Part I: Poisson and Stokes problems. J. Comput. Phys. 372*, 972–995.

[3] Zang, J., Ning, D., Liang, Q., Taylor, P., Borthwick, A., and Taylor, R. E. Modelling wave-coastal structure interactions using a cartesian cut cell method. In *Proceedings of IWWWFB22* (2007).

[4] Visbech, J., Engsig-Karup, A. P., and Ricchiuto, M. 2025. *A spectral element solution of the Poisson equation with shifted boundary polynomial corrections: influence of the surrogate to true boundary mapping and an asymptotically preserving Robin formulation.* J. Sci. Comput. 102(1), 11.

[5] Ciallella, M., Gaburro, E., Lorini, M., and Ricchiuto, M. 2023. *Shifted boundary polynomial corrections for compressible flows: high order on curved domains using linear meshes. Comput. Appl. Math. 441*, 127698.

[6] Engsig-Karup, A. P., Eskilsson, C., and Bigoni, D. 2016. *A stabilised nodal spectral element method for fully nonlinear water waves. J. Comput. Phys. 318*, 1–21.

[7] Wu, G. 1993. *Hydrodynamic forces on a submerged circular cylinder undergoing large-amplitude motion. J. Fluid Mech. 254*, 41–58.

[8] Engsig-Karup, A. P., Monteserin, C., and Eskilsson, C. 2019. *A Mixed Eulerian Lagrangian Spectral Element Method for Nonlinear Wave Interaction with Fixed Structures.* Water Waves 1(2), 315–342.

[9] Fenton, J. 1988. *The numerical solution of steady water wave problems.* Comput. Geosci. 14(3), 357–368.